Int. Journal of Refractory Metals and Hard Materials 61 (2016) 264–272

Contents lists available at ScienceDirect

Int. Journal of Refractory Metals and Hard Materials

journal homepage: www.elsevier.com/locate/IJRMHM

Cold rotary swaging of a tungsten heavy alloy: Numerical and experimental investigations

Radim Kocich [a], Lenka Kunčická [a,*], Daniel Dohnalík [b], Adéla Macháčková [a], Michal Šofer [c]

[a] Regional Materials Science and Technology Centre, VŠB TU Ostrava, 17. listopadu 15, 70833 Ostrava, Poruba, Czech Republic
[b] Department of Material Forming, Faculty of Metallurgy and Materials Engineering, VŠB TU Ostrava, 17. listopadu 15, 70833 Ostrava, Poruba, Czech Republic
[c] Faculty of Mechanical Engineering, VŠB – Technical University of Ostrava, Ostrava, Czech Republic

ARTICLE INFO

Article history:
Received 25 July 2016
Received in revised form 22 September 2016
Accepted 6 October 2016
Available online 08 October 2016

Keywords:
Rotary swaging
Tungsten heavy alloy
Finite element analysis
Texture
Mechanical properties

ABSTRACT

A finite element analysis was performed to predict behaviour of sintered tungsten-based heavy alloy during cold rotary swaging, while experimental investigations evaluated mechanical and structure properties in both, sintered and swaged material states. The simulation involved prediction of swaging force, which was subsequently compared with force measured experimentally using own designed force detection system, although other parameters, such as strain, strain rate, stress and temperature were also predicted and subsequently compared to experimental data. The results showed significant hardening and strengthening after swaging; the average ultimate strengths after sintering and swaging, respectively, were 860 MPa and 1680 MPa. This also contributed to very high swaging force of almost 600 kN. The distribution of microhardness across the cross-section confirmed the predicted strain distribution. Texture analyses revealed a notion of cube texture given primarily by the fcc matrix in the sintered state, while several ideal orientations for both the fcc and bcc phases were observed after swaging. As indicated by grains misorientations analyses, swaging introduced residual stress, the distribution of which was in conformity with the predicted stress and strain distributions.

1. Introduction

The favourable mechanical and physical properties determine the primary use of tungsten heavy alloys (THA) as radiation shielding and kinetic energy penetrators [1], although they can also be used to produce therapeutic radiators in oncology or as mass balances in aeronautics [2]. The alloys are usually fabricated from powder mixtures consisting of >90 wt% of tungsten grains and elements with lower melting points (Ni, Co, Fe etc.) usually dissolving between tungsten particles during sintering [3]. Although higher contents of W usually increase strength properties, contents of the binding phase lower than 3% generally decrease ductility, toughness and the ability to reduce porosity [4]. A typical THA production procedure consists of isostatic compression of powders, sintering at elevated temperatures, usually within the range of 1000–1500 °C, and subsequent deformation processing, advantageously via rotary swaging or drawing [4–6].

Rotary swaging (RS) is an intensive plastic deformation process gradually reducing cross-sections of work-pieces and increasing their lengths [7]. Due to its incremental character and favourable stress state, the method can advantageously be used to process pre-sintered materials. Favourable is also the prevailing shear deformation mechanism enabling elimination of residual porosity and additional structure refinement, as reported in various studies [8–12]. However, since the effect of strain is the highest on the work-piece surface and decreases towards its axis, RS introduces a certain cross-sectional inhomogeneity for relatively small overall strains.

RS can be performed under hot and cold conditions, depending on the swaged material, required surface quality and final properties. The influence of hot RS has already been reported e.g. for a WNiFe alloy [13]; this elemental composition has also already been subjected to cold swaging [14]. Nevertheless, the number of published works dealing with cold RS of THAs is very low. Moreover, study of background literature has not revealed any available report on the effects of cold rotary swaging on a WNiCo alloy. Cold processing is very favourable since it primarily increases strength via increasing dislocation density, which is especially important to increase durability of penetrators in military applications [3].

The aim of this study was to investigate the effects of cold rotary swaging on structure and properties of a WNiCo heavy alloy. A finite element analysis (FEA) was performed to investigate distributions of strain and strain rate, stress state, temperature and plastic flow, as well as to predict energy-power parameters and deformation behaviour of such hard to deform alloys. The experimental investigation consisted of measurement of energy-power parameters using an originally developed KOMAFU S600 force measuring system, as well as of analyses of mechanical properties, grain shapes and orientations, textures and grains misorientations indicating residual stresses for both the sintered

* Corresponding author.
E-mail address: lenka.kuncicka@vsb.cz (L. Kunčická).

http://dx.doi.org/10.1016/j.ijrmhm.2016.10.005
0263-4368/

and swaged material states. The experimental results were subsequently compared to the numerically predicted parameters.

2. Material and methods

2.1. FE analysis

Forge NxT commercial software was used to perform the simulation, the initial assembly for which consisted of four dies, a work-piece and a clamp bar used to push the work-piece forward each time the dies were open (Fig. 1a). During swaging, the dies oscillated in the radial direction and rotated around the swaging head axis after each stroke. The assembly was meshed with finite element meshes of tetrahedron elements; the mesh of the work-piece (initial diameter of 30 mm and length of 100 mm) consisted of 20,350 nodes. The initial temperature of the work-piece and dies was 20 °C, while friction between the dies and work-piece was determined via the Coulomb law with the friction coefficient of $\mu = 0.1$.

To define the material behaviour, a constitutive model was created on the basis of a stress-strain curve gained from a tensile test of the sintered material. Material behaviour was finally described by an elastic-viscoplastic model characterized by the Haensel–Spittel equation (Eq.(1)) having the advantage of counting with possible occurrence of softening processes over other equations used to analyse deformation under cold conditions (e.g. power law) [15,16].

$$\sigma = A\exp(m_1 T)T^{(m_9)}\varepsilon^{(m_2)}\exp\left(\frac{m_4}{\varepsilon}\right)(1+\varepsilon)^{(m_5 T)}\exp\left(m_7\varepsilon\right)\dot{\varepsilon}^{(m_3)}\dot{\varepsilon}^{(m_8 T)} \quad (1)$$

where ε is equivalent strain, $\dot{\varepsilon}$ is equivalent strain rate, T is temperature and A, m_1, m_2, m_3, m_4, m_5, m_6, m_7, m_8, m_9 are regression coefficients, the values of which were defined as follows: $A = 1447.002738$, $m_1 = -0.009$, $m_2 = 0.0895$, $m_3 = 0.0044$, $m_4 = -0.0069$, m_5, m_6, m_7, m_8, m_9 were equal to 0. The supplementary initial conditions ensuing from the model were Poisson coefficient of 0.3, specific heat of 130 $J\cdot kg^{-1}\cdot K^{-1}$, density of 19.3 $g\cdot cm^{-3}$, thermal conductivity of 173 $W\cdot m^{-1}\cdot K^{-1}$ and emissivity of 0.88. The model was valid within the temperature range of 20–350 °C, strain range of 0.04–2 and strain rate range of 0.01–500 s^{-1}.

2.2. Experimental material

Preparation of the initial powder mixture, as well as cold isostatic compression at 400 MPa, pre-sintering at 1540 °C and final annealing and quenching were carried out at UJP Praha a.s. The chemical composition of the sintered alloy is shown in Table 1.

After taking samples for subsequent analyses, the sintered material was subjected to a single pass cold swaging (Fig. 1b). The deformation degree calculated using Eq. (2), where S_0 is the initial and S_1 the final cross-section, was 0.36. Energy-power parameters (deformation force, deformation work) were recorded during the entire experiment. For this purpose we used the recently developed KOMAFU S600 system for dynamic force measurement [17].

Table 1
Chemical composition of WNiCo alloy.

Element	Content [wt%]	
	Matrix	Overall
W	43.11	92.62
Ni	37.97	4.98
Co	18.92	2.40

$$\varphi = \ln\frac{S_0}{S_1} \quad (2)$$

Samples of both the material states were subsequently subjected to Scanning Electron Microscopy (SEM), Vickers microhardness measurements and tensile testing. Microhardness was measured with 100 N load and 15 s indentation time for both the phases in multiple locations across the work-piece cross-section to enable calculation of individual average values as well as depiction of its distribution. Tensile properties were analysed with 0.5 mm/min cross-head velocity (0.56×10^{-3} s^{-1} strain rate) for both the material states, while two locations, the axial region and 2 mm below the work-piece surface, were analysed in the swaged state. The samples were prepared according to the ASTM E8/E8M standard with the working length of 50 mm. The used devices were a FMARS 900 (Future Tech) microhardness testing device with a diamond indenter and an Instron 3382 tensile testing machine.

As for SEM, EDX chemical composition analyses were performed using a Quanta FEG 450 SEM device at VŠB – TUO (Table 1), while EBSD scans for grains and texture observations were made using a Tescan Lyra 3 FIB/SEM with a NordlysNano EBSD detector at ASCR. To evaluate the scans, we used ImageJ [18], JTex [19], ATOM [20] and Channel5 [21] software.

3. Results and discussion

3.1. Numerical simulation

3.1.1. Imposed strain and strain rate

The predicted imposed strain distribution along a longitudinal work-piece cutting plane is shown in Fig. 2a. The highest effective strain of ~0.5 experienced the work-piece surface, although swaging affected the axial region, too. Strain gradually decreased towards the work-piece axis to the distance of approximately 6 mm below the surface, from which it kept a more or less constant value of ~0.25. The average imposed strain within the work-piece was then 0.284. The strain distribution across the work-piece cross-section is comparable to results of experiments reporting swaging with deformation degrees of 0.26 and 0.38 [22]; inhomogeneity of the imposed strain in the radial direction as well as a certain inhomogeneity in the axial direction are also comparable. However, when compared the deformation degree herein calculated using Eq. (2) (0.36), and the predicted average imposed strain (0.284), the calculated deformation degree is higher. This can be attributed to a quite low formability and high density of the sintered material,

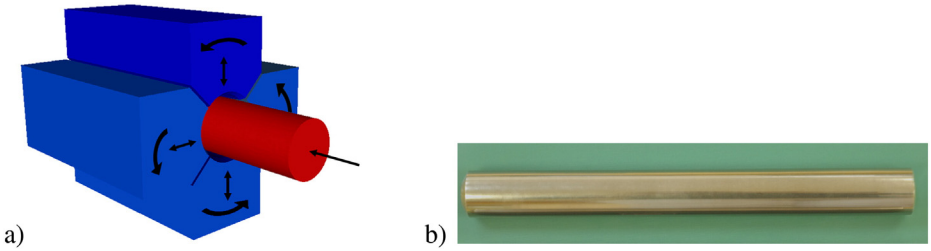

Fig. 1. (a) Set-up of assembly for numerical simulation; (b) final cold-swaged product.